Nanoscale Advances

ROYAL SOCIETY OF CHEMISTRY

PAPER

View Article Online
View Journal | View Issue

Cite this: *Nanoscale Adv.*, 2021, **3**, 2598

Pentacene/perfluoropentacene bilayers on Au(111) and Cu(111): impact of organic–metal coupling strength on molecular structure formation†

Qi Wang, [ab] Jiacheng Yang,[b] Antoni Franco-Cañellas, [a] Christoph Bürker,[a] Jens Niederhausen, [c] Pierre Dombrowski, [d] Felix Widdascheck, [d] Tobias Breuer, [d] Gregor Witte, [d] Alexander Gerlach, *[a] Steffen Duhm *[b] and Frank Schreiber [a]

As crucial element in organic opto-electronic devices, heterostructures are of pivotal importance. In this context, a comprehensive study of the properties on a simplified model system of a donor–acceptor (D–A) bilayer structure is presented, using ultraviolet photoelectron spectroscopy (UPS), X-ray photoelectron spectroscopy (XPS), low-energy electron diffraction (LEED) and normal-incidence X-ray standing wave (NIXSW) measurements. Pentacene (PEN) as donor and perfluoropentacene (PFP) as acceptor material are chosen to produce bilayer structures on Au(111) and Cu(111) by sequential monolayer deposition of the two materials. By comparing the adsorption behavior of PEN/PFP bilayers on such weakly and strongly interacting substrates, it is found that: (i) the adsorption distance of the first layer (PEN or PFP) indicates physisorption on Au(111), (ii) the characteristics of the bilayer structure on Au(111) are (almost) independent of the deposition sequence, and hence, (iii) in both cases a mixed bilayer is formed on the Au substrate. This is in striking contrast to PFP/PEN bilayers on Cu(111), where strong chemisorption pins PEN molecules to the metal surface and no intermixing is induced by subsequent PFP deposition. The results illustrate the strong tendency of PEN and PFP molecules to mix, which has important implications for the fabrication of PEN/PFP heterojunctions.

Received 16th January 2021
Accepted 8th March 2021

DOI: 10.1039/d1na00040c

rsc.li/nanoscale-advances

1. Introduction

Conjugated organic materials (COMs) have received considerable attention due to their potential for the application as active layers in novel (opto-)electronic devices, such as organic light emitting diodes (OLEDs) or organic photovoltaics (OPVs).[1–4] In particular, interface properties are of importance since they determine injection barriers and the energy level alignment (ELA) between an active material layer and the metal electrode.[5,6] Primer layers between the metal electrode and the organic semiconductor have been proven to be an efficient way for engineering interface energetics and tuning energy barriers for charge carrier injection/extraction.[7–9] Therefore, the interface between the active molecular layer and the metal substrate plays a crucial role as it is the key component of the organic film and hence will influence the performance in respective applications.[10–12] As shown in various studies, the coupling strength of the contact layer with the substrate, a factor which is crucial for the growth of subsequently deposited organic layers,[13–17] can be quantified through different experimental "indicators", *i.e.* vacuum-level shifts determined by ultraviolet photoelectron spectroscopy (UPS), core-level shifts determined by X-ray photoelectron spectroscopy (XPS) and bonding distances determined by the X-ray standing waves (XSW) technique.[18]

Being an intensively studied p-type semiconductor material, pentacene (PEN, $C_{22}H_{14}$) holds great potential for application as model system in organic electronic devices due to its good processability compared to smaller oligoacenes, and high charge carrier mobilities consistently reported for thin films.[19–23] With regard to the fabrication of (opto)electronics, a corresponding n-type organic semiconductor should have similar physical and structural properties except for the type of charge carriers.[24–27] For that reason, we chose perfluoropentacene (PFP, $C_{22}F_{14}$)[28–30] as acceptor material and studied the adsorption behavior and coupling strength between the two COMs. Mixed thin films based on this donor–acceptor

[a]*Institut für Angewandte Physik, Universität Tübingen, 72076, Tübingen, Germany. E-mail: alexander.gerlach@uni-tuebingen.de*

[b]*Institute of Functional Nano & Soft Materials (FUNSOM), Jiangsu Key Laboratory for Carbon-Based Functional Materials & Devices and Joint International Research Laboratory of Carbon-Based Functional Materials and Devices, Soochow University, Suzhou, 215123, People's Republic of China. E-mail: duhm@suda.edu.cn*

[c]*Helmholtz Zentrum Berlin für Materialien und Energie GmbH, 14109 Berlin, Germany*

[d]*Fachbereich Physik, Philipps-Universität Marburg, 35032, Marburg, Germany*

† Electronic supplementary information (ESI) available: Comparison of the bilayer LEED patterns; UPS full spectra; coverage-dependent vacuum level spectra; XSW results of PFP/PEN bilayer on Cu(111) (PDF). See 10.1039/d1na00040c

(D–A) pair have already been studied with optical methods, X-ray diffraction and theoretical methods demonstrating their structural compatibility and favorable electronic properties.[31–36] However, some fundamental properties of the first layers, in particular vertical bonding distances within a PEN/PFP heterostructure, have not been resolved, also because previous studies mostly used SiO_2 or HOPG as substrates, *i.e.* inert surfaces with weak interaction and/or limited usability for XSW measurements.[37,38] Specifically, the XSW and low-energy electron diffraction (LEED) technique require highly ordered and crystalline substrates, for instance, coinage metal single crystals, which can be easily prepared under ultrahigh vacuum (UHV) conditions, and also facilitate high resolution UPS and XPS measurements.[39–41] Therefore, we chose Au(111) and, for comparison, Cu(111) to study the two bilayer systems (PFP/PEN and PEN/PFP) on these substrates to elucidate the impact of the substrate interaction for this prominent D–A pair.

Below we will show that there is a significant difference in the ordering behavior employing either the strongly chemisorbed PEN/Cu(111)[42,43] or the physisorbed (PEN or PFP)/Au(111)[44,45] as basis for the molecular bilayer. Thereby, we demonstrate that such substrate induced effects can be highly relevant in the field of COMs on metals[46,47] as they also influence the electronic properties beyond the first layer.

2. Experimental methods

The high-resolution XPS (HR-XPS) and normal-incidence XSW (NIXSW) measurements on Au(111) have been carried out at beamline I09 at Diamond Light Source (DLS, UK) using the available soft (110–1100 eV) and hard (2.1–18 keV) X-ray beams.[48,49] Sample preparation and measurements were performed *in situ* under UHV conditions. The analysis chamber (base pressure: 3×10^{-10} mbar) features a VG Scienta EW4000 HAXPES hemispherical photoelectron analyzer, which is mounted at 90° relative to the incident X-ray beam. The XSW data on Cu(111) have been measured at beamline ID32 at European Synchrotron Radiation Facility (ESRF, France) using the HAXPES chamber with a SPECS PHOIBOS 225 HV hemispherical photoelectron analyzer.[50] The reflectivity and photoelectron core-level spectra of all elements were recorded at different photon energies typically within a ±3 eV interval around the Bragg energy (E_{Bragg}), *i.e.* ~2.63 keV for Au(111) and ~2.97 keV for Cu(111). The photoelectron yield (Y_P) and the reflectivity were modeled taking into account the experimental geometry and the non-dipole corrections associated with it.[51–53] The substrate was cleaned by several cycles of Ar^+ ion bombardment and annealing (400–500 °C). The COMs were sublimated onto the single-crystal surface (held at room temperature, or with sufficient waiting time after the desorption process of multilayers) by physical vapor deposition from home-built, resistively heated cells with deposition rates of about ~0.2 Å min^{-1}. The mass-related thickness was monitored by a quartz-crystal microbalance (QCM) positioned near the sample.

Thickness-dependent UPS measurements were carried out at Soochow University in a UHV system consisting of three interconnected chambers: an evaporation chamber (base pressure: 3×10^{-10} mbar), an annealing and sputtering chamber (3×10^{-10} mbar) and an analysis chamber (base pressure: 2×10^{-10} mbar). UPS experiments were performed using monochromatized He I radiation (21.22 eV) and a SPECS PHOIBOS 150 analyzer. The energy resolution was 80 meV. The angle between the incident beam and the sample was fixed to 40°. The spectra were collected at photoelectron take-off angles (θ) of 45° with an acceptance angle of ±12° along the ⟨11−2⟩ azimuthal direction of Au(111). A sketch of the measurement geometry can be found in ref. 42. The secondary electron cut-off (SECO) (to determine the vacuum level) was measured in normal emission with a bias potential of −3 V. Low-energy electron diffraction (LEED) was performed using a Micro-Channel-Plate LEED (OCI BDL800IR-MCP) which is installed in the analysis chamber. The LEED patterns were recorded using typical electron beam energies E_{kin} <30 eV. LEED pattern simulations were done using the LEEDpat[54] software. All measurements have been performed at room temperature (295 K).

3. Results and discussion

The PEN and PFP monolayers as well as the bilayer heterostructures have been prepared by organic molecular beam deposition (OMBD),[55] and were characterized by HR-XPS, XSW, LEED and UPS. Well-defined molecular monolayers of the unitary films on the metal substrates were obtained by initially growing thin multilayers (~10 Å) and afterwards carefully heating them at 420 K to selectively desorb excessing multilayers. In the second step, submonolayers of the complementary acene have been deposited on the annealed sample.

3.1 Monolayer characterization on Au(111)

Before performing XSW measurements, the XPS signatures of both pristine acene films have to be determined. Single-component monolayer data of PEN and PFP, respectively, are displayed in Fig. 1, *i.e.* C 1s and F 1s core-level spectra and the corresponding photoelectron yield (Y_P) curves. As shown in Fig. 1a, the C 1s signal of PEN is located at a binding energy (BE) of 284.15 eV, which agrees well with previous studies.[56,57] In Fig. 1b, C 1s and F 1s core-level data of PFP and a corresponding fit are shown, together with basic Voigt profiles. We find the fluorine signal of PFP at a BE of 687.07 eV. For the C 1s core-level spectra, different contributions are considered as illustrated by the color code used in its chemical structure (*cf.* inset in Fig. 1a, b). The two main peaks are attributed to the carbon signals of PFP with an intensity ratio that corresponds to the stoichiometry of the molecule. While the peak with an area ratio of ~35% at 284.87 eV is related to carbon atoms within C–C bonds, the peak at 286.49 eV (~53%) is related to the fluorinated carbon atoms (C–F).[43,58] In addition, the shoulder (~6%) at the higher BE side (~290 eV) of the carbon C–F feature is attributed to shake-up satellites,[59,60] whereas the other shoulder at lower BE (~283 eV) is attributed to a small fraction (~5%) of broken C–F bonds and the respective C atoms bound to the metal substrate.[61,62] The carbon peak positions will further be used to

distinguish different carbon species in the XPS bilayer spectra, which allows to measure adsorption distances for both molecules separately.

Using the NIXSW technique, we have measured C 1s and F 1s core-level spectra at photon energies close to the Bragg energy of the Au(111) reflection (2.634 keV). The XP spectra were recorded at 31 different photon energies around the Bragg energy of the gold substrate, and each spectrum is fitted by applying the profiles adapted from HR-XPS results. The resulting photoelectron yield curves as a function of photon energy, obtained from the intensity of the core-level signals, are shown in Fig. 1. By fitting these photoelectron curves together with the substrate reflectivity two parameters are obtained, which provide structural information of the adsorbates. On the one hand, the coherent position P_H ($0 \leq P_H \leq 1$), which is directly related to the adsorption distance for a given chemical species *via* $d_H = d_0(n + P_H)$,[63] where $d_0 = 2.35$ Å is the lattice plane spacing of the gold crystal along the H = [111] direction (with n being an integer number to be chosen depending on the circumstances, *c.f.* modulo-d ambiguity). On the other hand, the coherent fraction f_H ($0 \leq f_H \leq 1$), which contains the information about the vertical ordering of a given species around its mean adsorption distance ($f_H = 0$ for totally disordered ensembles and $f_H = 1$ for the case that the atoms are all at the same adsorption distance). This procedure allows us to determine the precise adsorption distances (typically within an error bar of about 0.05 Å (ref. 64)) of all four relevant atomic species (C in PEN, two species of C in PFP: C–C, C–F, as well as F). To consider the surface relaxation of Au, the values were corrected as explained in ref. 65.

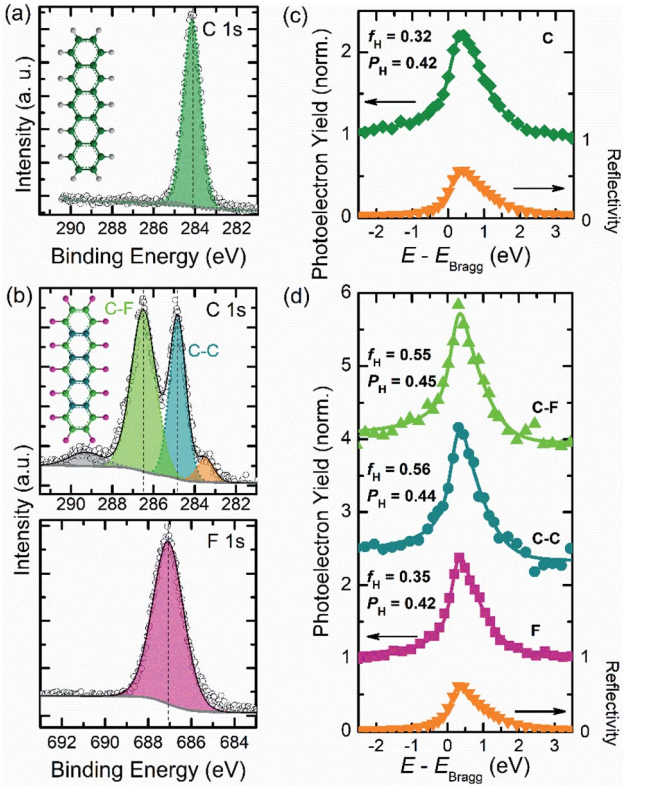

Fig. 1 XPS results of (a) C 1s core-level spectrum of monolayer PEN on Au(111); (b) C 1s and F 1s core-level spectra of monolayer PFP on Au(111), with chemical structures inserted, $h\nu = 800$ eV. XSW photoelectron yield (Y_P) results of PEN (c), PFP (d) monolayer adsorbed on the Au(111) substrate. At the bottom of (c) and (d), typical reflectivity curves for Au(111) surfaces are shown as orange curves. On the top of (c) and (d), Y_P of specific components is included. The structural information is contained in the coherent position, P_H, and the coherent fraction, f_H. The chemical sensitivity of this technique provides information for the different atom species, carbon and fluorine, as well as for the different inequivalent carbon atoms in PFP (named as C–C and C–F). Spectra are taken around the Bragg energy $E_{Bragg} = 2.634$ keV of Au(111). The color code of each curve in XPS and XSW figures corresponds to the color in the chemical structures shown in the insets in (a, b).

We are able to directly evaluate the adsorption distances of PEN and PFP, respectively, on the Au substrate (see Fig. 1c, d). The coherent position $P_H = 0.42$ obtained for PEN on Au(111) (Fig. 1c) corresponds to a distance $d_H = 3.28$ Å, which is clearly within the range of adsorption distances of physisorbed COMs on this substrate.[48,66,67] We note that the measured d_H is much larger than that of PEN on Cu(111) (2.34 Å) where PEN is chemisorbed.[43] Compared to a PEN monolayer on Au(111), PFP (Fig. 1d) has a very similar adsorption distance with its fluorine atoms located at a distance $d_H = 3.28$ Å ($P_H = 0.42$) and both carbon species ($P_H = 0.45$) at 0.05 Å higher adsorption distance than fluorine. Since the 0.05 Å difference found here is within the error margin of the NIXSW measurements and because of the relatively weak interaction with the substrate, we propose an essentially flat adsorption geometry of PFP molecules on Au(111). A similar finding has been reported also for PFP on Ag(111),[68] in contrast to PFP on Cu(111) where the carbon atoms are found *below* the fluorine.[43] The coherent fractions (f_H) obtained for both carbon species of PFP (0.56 and 0.55), indicate decent vertical order of the carbon atoms in PFP.[69] This parameter, however, is smaller for the F 1s signal ($f_H = 0.35$) in Fig. 1d, which implies a larger spread in adsorption distances of fluorine atoms. Overall, we can conclude that for PEN and PFP monolayers on Au(111) the molecules are essentially flat-lying with adsorption distances that are typical for physisorbed COMs, which is consistent with previous near-edge X-ray absorption fine structure studies.[70,71]

The information of well defined monolayer films is confirmed by distinct LEED patterns for PEN and PFP on Au(111), that also allows to determine the in-plane structure of these systems (see Fig. S1† for a detailed analysis). Thereby, we find that the unit cell parameters of both monolayers agree with previous reports.[42,72]

3.2 Bilayer characterization

To characterize the electronic properties of the two bilayers on the Au substrate, HR-XPS measurements have been carried out to extract the molecular core-level information and to enable the structural analysis by means of XSW. To avoid the formation of multilayer islands during deposition of the second component on the full monolayer of the first component, only a submonolayer (about 80% of a monolayer) was deposited as the second layer. As shown in Fig. 2, the two growth sequences of the bilayers, *i.e.* deposition of a (sub-)

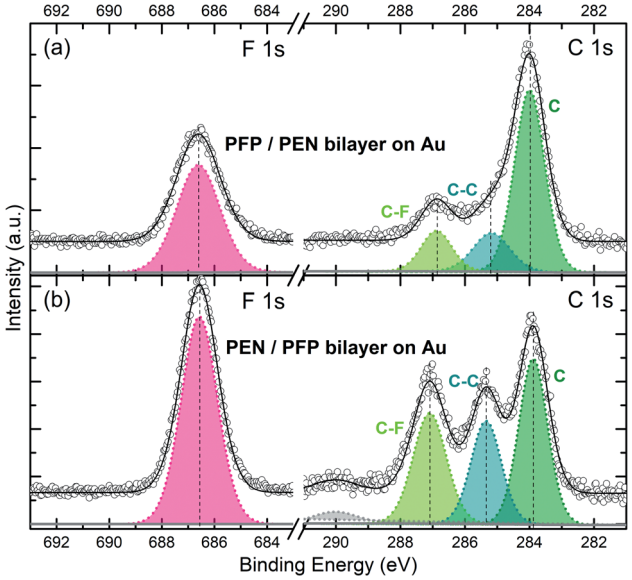

Fig. 2 HR-XPS results of bilayers on Au(111). (a) PFP deposited on a PEN monolayer on Au(111); (b) PEN deposited on a PFP monolayer on Au(111). Dashed vertical lines denote peak positions.

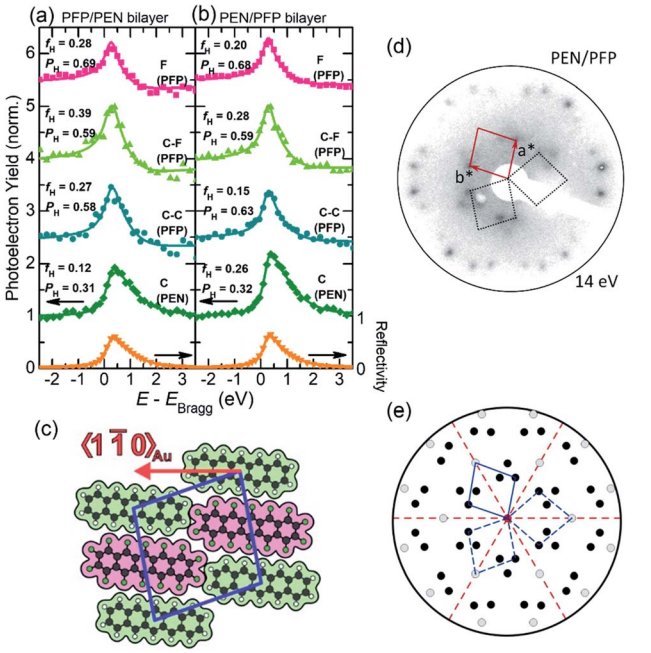

Fig. 3 (a) and (b) XSW fitting results of the D–A bilayers adsorbed on the Au(111) substrate. The structural information is contained within the coherent position, P_H, and the coherent fraction, f_H. Spectra are taken around the Bragg energy $E_{Bragg} = 2.634$ keV of Au(111). (c) Model of a mixed film with the unit cell derived from the LEED pattern, (d) measured LEED pattern of a nominal PEN/PFP bilayer on Au(111), (e) simulated LEED pattern. Red dashed lines indicate the ⟨11–2⟩ azimuth directions of the substrate, unit cells are marked in blue, black dots mark experimentally observed spots and gray ones are not observed.

monolayer PEN on a monolayer PFP on Au(111) and *vice versa*, result in nearly identical binding energies of the core-level signals and the equivalent chemical sub-levels. As expected, in both cases, the top layers show somewhat lower intensities as slightly less than one monolayer has been deposited. In Fig. 2a, the F 1s signal at a BE of 686.55 eV originating from the PFP molecules in the bilayer is at 0.52 eV lower BE than in the PFP monolayer (Fig. 1b). Interestingly, the carbon core-level spectra reveal three distinct peaks at 284.01 eV (67.3%), 285.18 eV (17.4%) and 286.88 eV (15.3%) as depicted in Fig. 2a. The prominent peak at the lowest BE, which is associated with PEN molecules in the bilayer, is observed at lower BE ($\Delta = -0.14$ eV compared to the PEN monolayer on Au(111) in Fig. 1a). The two peaks with similar intensities at higher BE are attributed to C–C and C–F contributions of PFP molecules in the bilayer. The C–C peak of PFP is shifted to higher BE ($\Delta = +0.31$ eV compared to the PFP monolayer spectrum on Au), *i.e.* contrary to the PEN carbon signal, as well as the C–F peak of PFP ($\Delta = +0.39$ eV). Importantly, for the PEN on PFP bilayer spectrum shown in Fig. 2b the three main peaks, which correspond to the same chemical species as just discussed, exhibit the same trend of core-level shifts as the PFP on PEN bilayer: The C 1s signal derived from PEN (39.4%) is located at an even lower BE ($\Delta = -0.26$ eV), while the C–C (25.8%) and C–F (30.4%) signals of PFP shift to higher BE ($\Delta = +0.47$ and +0.59 eV). The specific values of these peak positions, which are summarized in Table S1,† indicate a notable interaction of both acene molecules in the bilayer. The impact of this pronounced electronic effect on the energy levels in the valence band of PEN/PFP bilayers will be discussed below based on the UPS measurements for these systems.

The XSW bilayer data displayed in Fig. 3a, b are derived using the various peak positions identified afore in the HR-XPS spectra (Fig. 2) to extract the photoelectron yield (Y_P), obtained for slightly different incident X-ray beam energies. Hence, we are able to provide structural information for each element and chemically inequivalent species of PEN and PFP. For the two bilayer systems considered, *i.e.* PFP on PEN (Fig. 3a) and PEN on PFP (Fig. 3b), robust coherent positions and fractions could be derived for all carbon species and the fluorine atoms. The fluorine signal, which is necessarily related to the PFP molecules, apparently yields an adsorption distance of PFP 6.23 Å ($P_H = 0.69$) above the Au(111) surface within the PFP/PEN bilayer. Interestingly, the fluorine signal is practically the same for the PEN/PFP bilayer with almost identical P_H and similar f_H values. Further insight into the adsorption behavior can be derived from the carbon species of PEN and PFP: For both bilayers, we find nearly identical coherent positions P_H for C (PEN) with 0.31 *vs.* 0.32, and likewise for C–C and C–F (PFP) values close to 0.60. Thus, the coherent positions for all species are within the error margin independent of the deposition sequence. Moreover, they are significantly different from the respective values of the monolayer systems (*cf.* Table 1). In principle, this could be explained by bilayer formation and with the bonding distance of the molecules in the contact layer (first monolayer) being strongly affected by the adsorption of the second layer. Another possible scenario, however, is partial molecular exchange in a way that, for both systems, PEN as well as PFP molecules occupy the first and the second layer with

Table 1 Coherent fractions (f_H), coherent positions (P_H) and vertical adsorption distances (d_H [Å]) obtained by XSW measurements, *i.e.* for monolayers of PEN and PFP on Au(111), bilayer systems of PFP on PEN and PEN on PFP on Au(111), monolayers of PEN on Cu(111) and PFP/PEN bilayers on Cu(111), respectively

		Au(111)					Cu(111)	
		PEN	PFP	PFP/PEN	PEN/PFP		PEN	PFP/PEN
C (PEN)	f_H	0.32	—	0.12	0.26	C (PEN)	0.52	0.40
	P_H	0.42	—	0.31	0.32		0.16	0.13
	d_H	3.28(0)	—	—	—		2.43	2.35
C–C (PFP)	f_H	—	0.56	0.27	0.15	C (PFP)	—	0.21
	P_H	—	0.44	0.58	0.63			
	d_H	—	3.33(2)	—	—		—	0.79
C–F (PFP)	f_H	—	0.55	0.39	0.28			
	P_H	—	0.45	0.59	0.59		—	5.73
	d_H	—	3.33(1)	—	—			
F 1s	f_H	—	0.35	0.28	0.20	F 1s	—	0.20
	P_H	—	0.42	0.69	0.68		—	0.69
	d_H	—	3.28(2)	—	—		—	5.54

similar probability, which means that mixed bilayers are formed. The modulo-*d* ambiguity of NIXSW complicates an assignment of vertical bonding distances in heterostructures.[63] Nevertheless, for a bilayer with PFP exclusively in the contact layer on Au(111), *i.e.* without considering a mixed bilayer, the coherent position that was measured would correspond to adsorption distances either in the range of ~1.4 Å or ~3.7 Å (calculation see Table S2†), which are both unreasonable values, *e.g.* too small or too large considering conventional molecular layers on gold. For PEN in the contact layer, an average adsorption height of ~3.0 Å would be obtained, which is in the range of reasonable values for COMs on Au(111).[48] Yet, the adsorption distances of PEN in both bilayers would be rather low compared to its monolayer value of 3.28 Å on Au(111), considering that for other bilayer systems on Au(111) the second layer does not influence the adsorption distance of the first layer significantly.[73] Therefore, we conclude that the most likely reason for such unreasonable adsorption heights and the observed small coherent fractions, compared to an ordered bilayer as *e.g.* F_{16}CuPc/PTCDI on Au(111) with $f_H \approx 0.5$,[73] is that PEN and PFP molecules occupy both layers of the bilayer systems due to strong intermixing.

To characterize the lateral molecular arrangement in the bilayer films, we have conducted LEED measurements on bilayer heterostructures of PEN and PFP. The analysis of the PEN/PFP bilayer LEED pattern is shown in Fig. 3c–e. From the experimental LEED pattern (Fig. 3d), a $\begin{pmatrix} 6 & -2 \\ -2 & 6 \end{pmatrix}$ superstructure has been derived, showing that the corresponding unit cell is significantly larger than that of the monolayer films on Au(111) (Fig. S1†) with $a = 15.29$ Å, $b = 15.29$ Å and $\gamma = 81.8°$. In particular, b is increased by a factor of ~2 in comparison to the unit cell of the pristine monolayers, so that a and b are now equal, which allows us to conclude that the unit cell contains two acene molecules. Since identical LEED patterns for both stacking sequences have been observed (*i.e.* PEN/PFP and PFP/PEN, Fig. S2†), it indicates that in each case the unit cell contains two different molecules which can be attributed to PEN and PFP, respectively. The corresponding molecular superstructure is illustrated in Fig. 3c. Notably, such a lateral arrangement proposed for the mixed bilayer was found recently also for a mixed PEN:PFP monolayer film on MoS_2.[74]

Further support for this intermixing scenario comes from a comparison with the PFP/PEN bilayer on Cu(111). In this heterostructure the adsorption behavior is strongly influenced by the molecule–substrate interaction and bilayer formation (in contrast to intermixing) can be expected.[18,75] PEN monolayers on Cu(111) are chemisorbed[42,76] and the measured adsorption distance (Table 1; photoelectron yield curves in Fig. S5†) is much lower than that on Au(111), which is in full agreement with previous reports.[43,77] As indicated by the coherent fractions, PEN monolayers on Cu(111) also exhibit a higher (vertical) order than on Au(111) ($f_H = 0.52$ compared to $f_H = 0.31$). For a more detailed discussion of the PEN monolayer on Cu(111) we refer to ref. 43, which furthermore compares the adsorption behavior with that of PFP.

For the PFP/PEN bilayer on Cu(111) the C 1s signals of both molecules can be distinguished in the XSW measurement, see Fig. S5†(d). Having fitted the data, the coherent positions P_H translate into reasonable vertical adsorption heights (Table 1): The adsorption distance d_H of PEN changes only slightly ($\Delta = -0.08$ Å) from the monolayer to the bilayer system and the PEN–PFP molecular distance (3.38 Å) agrees with the vertical stacking distance in the PEN/PFP co-crystal.[78] Comparing these results with other bilayers, *i.e.* CuPc/P4O on Ag(111)[18] and F_{16}CuPc/PTCDI on Au(111),[73] shows that the characteristic adsorption distance between two organic molecular layers is ~3.3 Å and that in ordered bilayers, the second layer mostly physisorbs on the first COM layer (more details in Fig. S5† and Table 1). In particular, the molecules with strong donor character tend to move closer to the substrate, whereas those with an acceptor (or weaker donor) behavior tend to move away from it.[18,79,80] We note that due to chemical interactions PFP molecules on Cu(111) have a disposition to thermally induced defluorination,[70] which does not allow a controlled thermal desorption of

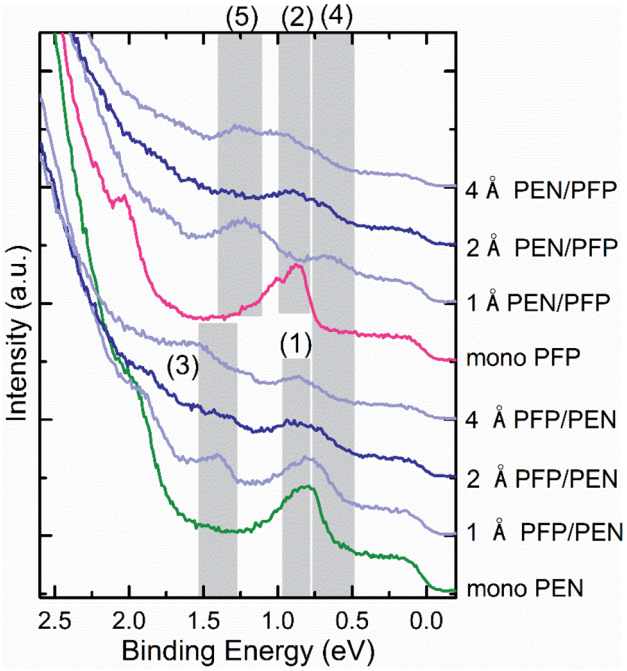

Fig. 4 UP spectra for subsequently deposited layers of PEN and PFP on Au(111). The green curve corresponds to the PEN monolayer, the pink curve to the PFP monolayer, the blue curves to the mixture and the darker blue curves to the bilayers. Survey spectra of these systems can be found in Fig. S3 of the ESI.†

excessing PFP multilayers and thus hampers a reliable preparation of PEN/PFP bilayers on Cu(111).

In order to characterize the valence band structure of the bilayers on Au(111), we performed UPS measurements. Corresponding spectra for different PEN + PFP heterostructures and thicknesses are shown in Fig. 4. Here, the labels only refer to the deposition order and not to the real situation on the surface. It is known from literature that the HOMO-derived peak of PEN and PFP monolayers on Au(111) are centered at 0.78 eV BE and 0.90 eV BE, respectively.[42,45] This agrees well with our data of the monomolecular systems, where the HOMO-derived peaks are centered at 0.79 eV for PEN (feature 1) and 0.85 eV for PFP (feature 2), respectively. Upon deposition of PFP on top of the PEN monolayer, the intensity of this peak is decreasing and a new peak (feature 3) appears, which is located at a similar BE as the HOMO-level of PFP in multilayers on Au(111).[45] The other new features (4 and 5) of the heterostructures cannot be related to any peak of thickness-dependent PEN or PFP spectra on Au(111).[42,45] However, similar features have been observed for a mixed PEN:PFP thin film on HOPG and could be related to the interplay of induction, electrostatic and substrate contribution to polarization energies.[78] Overall, the UPS data supports, thus, the conclusion of mixed bilayer formation. A detailed discussion of the valence electronic structure, however, would require precise knowledge of the thin film structure and is beyond the scope of this study.

4. Conclusion

The results of the present work are schematically summarized in Fig. 5, *i.e.* the monolayer adsorption geometry with the element-specific adsorption distances of both molecules, a possible arrangement of PEN and PFP molecules in the mixed bilayer phase, and the observed core-level shifts in the mixtures. As discussed above, the monolayers of PEN and PFP on Au(111) are structurally well defined (see Fig. 5a) with typical physisorption distances of 3.28 Å for PEN and 3.32 Å for PFP as determined by the XSW measurements. Due to the strong chemisorption of PEN on Cu(111) (2.35 Å), sequential bilayer growth of PFP and PEN is facilitated on this substrate. The measured PFP-PEN distance of 3.38 Å on Cu(111), however, is typical for COMs interacting mostly *via* van der Waals forces. This can be compared to the experimental structure of PEN/PFP co-crystals[78] with an intermolecular spacing of 3.4 Å. In contrast, PEN–PFP bilayers grown on Au(111) form a laterally mixed phase, for which we suggest an alternate vertical stacking motif (Fig. 5c). For this, the C 1s core-level peaks of PEN (open symbols) shift to lower BE (−0.14 eV and −0.26 eV), while the two carbon species of PFP (solid symbols) shift to higher BE

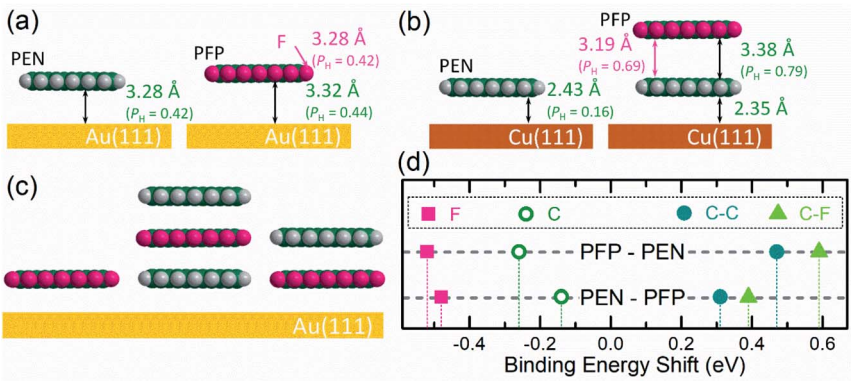

Fig. 5 Molecular growth model of (a) PEN and PFP monolayers on Au(111), (b) PEN monolayer and PFP/PEN bilayer on Cu(111). The adsorption distances derived from XSW measurements are included. Pink values belong to the fluorine atoms and green to the carbon atoms. (c) Schematic of the suggested bilayer mixture on Au(111), (d) core-level shifts of PEN (hollow circles) and PFP (solid spots) in the bilayer mixtures on Au(111) with respect to the monolayer BE for the PEN and PFP molecules.

(approx. +0.5 eV). Notably, in both systems the F 1s signals, *i.e.* those corresponding to the strongly electro-negative species, shift by the same amount towards lower BE (approx. −0.5 eV).

As discussed above, both PEN–PFP bilayer systems on Au(111) feature a 1 : 1-mixed phase, *i.e.* similar to PEN : PFP monolayers on MoS_2 (ref. 74) and to PEN : PFP blends in thicker films.[81] We believe that the opposite electrostatic quadrupole moments of PEN and PFP[82–86] promote the reordering on Au(111) – quite similar to what was recently reported for PEN : PFP heterostructures on the weakly interacting HOPG substrate with a valence band structure resembling the one shown in Fig. 4 for Au(111).[78] Hence, considering the different structures emerging in the molecular bilayer system on different substrates we conclude that the mixed phase can form due to weaker molecule–substrate interactions as, for example, on Au(111). In contrast, for PEN and PFP bilayers grown on Cu(111) the strong molecule–substrate interaction suppresses a re-ordering and yields a uniform stacking structure on the surface. The strong coupling of a PEN monolayer with Cu(111) hinders molecular exchange and a well-defined heterointerface is formed upon deposition of PFP.

In summary, we have studied the structure and electronic properties of a typical conjugated D–A pair in bilayers on Au(111) and Cu(111) surfaces using XSW, LEED, HR-XPS and UPS. The data consistently indicate mixture formation within the PEN : PFP bilayers on Au(111) with nearly identical properties for the two deposition sequences. Since the arrangement and order in organic heterostructures generally affects the performance of (opto-)electronic devices, the formation of mixed phases reduces device efficiency. Predicting the order in organic heterostructure is, thus, essential for rational device design. Our work shows that the intermixing tendency of PEN and PFP is quite strong and a chemisorbed first layer can be used to suppress this.

Author contributions

Q. W. has analysed the data and wrote the main paper as well as the ESI† with input from all co-authors. T. B., A. G. and F. S. have conceived and developed the idea and proposed the experimental plan. A. F-C., P. D., F. W. and A. G. have performed the HR-XPS and XSW measurements on Au(111). J. Y. and S. D. have performed the UPS measurements. C. B., J. N., A. G. and S. D. have performed the measurements on Cu(111). P. D., F. W. and G. W. analysed the LEED data. All authors discussed the results and their implications and commented on the manuscript at all stages.

Conflicts of interest

There are no conflicts to declare.

Acknowledgements

The authors thank the Diamond Light Source for access to beamline I09 and the European Synchrotron Radiation Facility for access to beamline ID32 and staff members, especially David A. Duncan (DLS) and Blanka Detlefs (ESRF) for excellent support during the beamtimes. Financial support from the Soochow University–Western University Center for Synchrotron Radiation Research, the Collaborative Innovation Center of Suzhou Nano Science & Technology (NANO-CIC), National Key R&D Program of China (No. 2017YFA0205002), 111 Project of the Chinese State Administration of Foreign Experts Affairs and the Deutsche Forschungsgemeinschaft (DFG) is gratefully acknowledged. Q. W. gratefully acknowledges financial support from the China Scholarship Council.

References

1 M.-K. Fung, Y.-Q. Li and L.-S. Liao, *Adv. Mater.*, 2016, **28**, 10381–10408.
2 O. Ostroverkhova, *Chem. Rev.*, 2016, **116**, 13279–13412.
3 R. S. Gurney, D. G. Lidzey and T. Wang, *Rep. Prog. Phys.*, 2019, **82**, 036601.
4 G. Schweicher, G. Garbay, R. Jouclas, F. Vibert, F. Devaux and Y. H. Geerts, *Adv. Mater.*, 2020, **32**, 1905909.
5 M. Gruenewald, C. Sauer, J. Peuker, M. Meissner, F. Sojka, A. Schöll, F. Reinert, R. Forker and T. Fritz, *Phys. Rev. B*, 2015, **91**, 155432.
6 M. Fahlman, S. Fabiano, V. Gueskine, D. Simon, M. Berggren and X. Crispin, *Nat. Rev. Mater.*, 2019, **4**, 627–650.
7 A. Tan and P. Zhang, *J. Phys.: Condens. Matter*, 2019, **31**, 503001.
8 X. Wu, R. Jia, J. Pan, X. Zhang and J. Jie, *Nanoscale Horiz.*, 2020, **5**, 454–472.
9 F. Widdascheck, A. A. Hauke and G. Witte, *Adv. Funct. Mater.*, 2019, **29**, 1808385.
10 A. Mänz, A. A. Hauke and G. Witte, *J. Phys. Chem. C*, 2018, **122**, 2165–2172.
11 X. Zhang, Z. Wang, X. Zhou, Z. Wang, L. Huang and L. Chi, *Adv. Electron. Mater.*, 2017, **3**, 1700128.
12 X. Yang, L. Egger, J. Fuchsberger, M. Unzog, D. Lüftner, F. Hajek, P. Hurdax, M. Jugovac, G. Zamborlini, V. Feyer, G. Koller, P. Puschnig, F. S. Tautz, M. G. Ramsey and S. Soubatch, *J. Phys. Chem. Lett.*, 2019, **10**, 6438–6445.
13 J. M. Gallego, D. Ecija, N. Martín, R. Otero and R. Miranda, *Chem. Commun.*, 2014, **50**, 9954–9957.
14 S. Thussing, L. Fernández and P. Jakob, *J. Phys.: Condens. Matter*, 2019, **31**, 134002.
15 B. Stadtmüller, S. Schröder, F. C. Bocquet, C. Henneke, C. Kleimann, S. Soubatch, M. Willenbockel, B. Detlefs, J. Zegenhagen, T.-L. Lee, F. S. Tautz and C. Kumpf, *Phys. Rev. B*, 2014, **89**, 161407.
16 R. Forker, M. Gruenewald, F. Sojka, J. Peuker, P. Mueller, C. Zwick, T. Huempfner, M. Meissner and T. Fritz, *J. Phys.: Condens. Matter*, 2019, **31**, 134004.
17 B. Stadtmüller, M. Gruenewald, J. Peuker, R. Forker, T. Fritz and C. Kumpf, *J. Phys. Chem. C*, 2014, **118**, 28592–28602.
18 Q. Wang, A. Franco-Cañellas, P. Ji, C. Bürker, R.-B. Wang, K. Broch, P. K. Thakur, T.-L. Lee, H. Zhang, A. Gerlach, L. Chi, S. Duhm and F. Schreiber, *J. Phys. Chem. C*, 2018, **122**, 9480–9490.

19 K. Broch, J. Dieterle, F. Branchi, N. J. Hestand, Y. Olivier, H. Tamura, C. Cruz, V. M. Nichols, A. Hinderhofer, D. Beljonne, F. C. Spano, G. Cerullo, C. J. Bardeen and F. Schreiber, *Nat. Commun.*, 2018, **9**, 954.
20 J. Lee, P. Jadhav, P. D. Reusswig, S. R. Yost, N. J. Thompson, D. N. Congreve, E. Hontz, T. Van Voorhis and M. A. Baldo, *Acc. Chem. Res.*, 2013, **46**, 1300–1311.
21 L. Zhao, R. I. Kaiser, W. Lu, M. Ahmed, M. M. Evseev, E. K. Bashkirov, V. N. Azyazov, C. Tçnshoff, F. Reicherter, H. F. Bettinger and A. M. Mebel, *Angew. Chem., Int. Ed.*, 2020, **59**, 1–6.
22 P. Hurdax, M. Hollerer, P. Puschnig, D. Lüftner, L. Egger, M. G. Ramsey and M. Sterrer, *Adv. Mater. Interfaces*, 2020, **7**, 2000592.
23 Y. Wakayama, D. G. de Oteyza, J. M. Garcia-Lastra and D. J. Mowbray, *ACS Nano*, 2011, **5**, 581–589.
24 F. Anger, J. O. Ossó, U. Heinemeyer, K. Broch, R. Scholz, A. Gerlach and F. Schreiber, *J. Chem. Phys.*, 2012, **136**, 054701.
25 J.-Q. Zhong, X. Qin, J.-L. Zhang, S. Kera, N. Ueno, A. T. S. Wee, J. Yang and W. Chen, *ACS Nano*, 2014, **8**, 1699–1707.
26 S. Hammer, C. Zeiser, M. Deutsch, B. Engels, K. Broch and J. Pflaum, *ACS Appl. Mater. Interfaces*, 2020, **12**, 53547–53556.
27 S. Kera, S. Hosoumi, K. Sato, H. Fukagawa, S.-i. Nagamatsu, Y. Sakamoto, T. Suzuki, H. Huang, W. Chen, A. T. S. Wee, V. Coropceanu and N. Ueno, *J. Phys. Chem. C*, 2013, **117**, 22428–22437.
28 A. Hinderhofer, T. Hosokai, C. Frank, J. Novák, A. Gerlach and F. Schreiber, *J. Phys. Chem. C*, 2011, **115**, 16155–16160.
29 Y. Sakamoto, T. Suzuki, M. Kobayashi, Y. Gao, Y. Fukai, Y. Inoue, F. Sato and S. Tokito, *J. Am. Chem. Soc.*, 2004, **126**, 8138–8140.
30 M. C. R. Delgado, K. R. Pigg, D. A. da Silva Filho, N. E. Gruhn, Y. Sakamoto, T. Suzuki, R. M. Osuna, J. Casado, V. Hernández, J. T. L. Navarrete, N. G. Martinelli, J. Cornil, R. S. Sánchez-Carrera, V. Coropceanu and J.-L. Brédas, *J. Am. Chem. Soc.*, 2009, **131**, 1502–1512.
31 T. Breuer and G. Witte, *J. Chem. Phys.*, 2013, **138**, 114901.
32 S. Duhm, I. Salzmann, G. Heimel, M. Oehzelt, A. Haase, R. L. Johnson, J. P. Rabe and N. Koch, *Appl. Phys. Lett.*, 2009, **94**, 033304.
33 Y. Nakayama, R. Tsuruta, N. Moriya, M. Hikasa, M. Meissner, T. Yamaguchi, Y. Mizuno, T. Suzuki, T. Koganezawa, T. Hosokai, T. Ueba and S. Kera, *J. Phys. Chem. Lett.*, 2019, **10**, 1312–1318.
34 V. O. Kim, K. Broch, V. Belova, Y. S. Chen, A. Gerlach, F. Schreiber, H. Tamura, R. G. Della Valle, G. D'Avino, I. Salzmann, D. Beljonne, A. Rao and R. Friend, *J. Chem. Phys.*, 2019, **151**, 164706.
35 A. Rinn, T. Breuer, J. Wiegand, M. Beck, J. Hübner, R. C. Döring, M. Oestreich, W. Heimbrodt, G. Witte and S. Chatterjee, *ACS Appl. Mater. Interfaces*, 2017, **9**, 42020–42028.
36 A. El-Sayed, D. J. Mowbray, J. M. García-Lastra, C. Rogero, E. Goiri, P. Borghetti, A. Turak, B. P. Doyle, M. Dell'Angela, L. Floreano, Y. Wakayama, A. Rubio, J. E. Ortega and D. G. de Oteyza, *J. Phys. Chem. C*, 2012, **116**, 4780–4785.
37 K. Vedam, *Surf. Sci.*, 1976, **56**, 221–236.
38 H. Fukagawa, H. Yamane, T. Kataoka, S. Kera, M. Nakamura, K. Kudo and N. Ueno, *Phys. Rev. B*, 2006, **73**, 245310.
39 H. Mönig, J. Sun, Y. M. Koroteev, G. Bihlmayer, J. Wells, E. V. Chulkov, K. Pohl and P. Hofmann, *Phys. Rev. B*, 2005, **72**, 085410.
40 N. Memmel, *Surf. Sci. Rep.*, 1998, **32**, 91–163.
41 D. P. Woodruff, *Rep. Prog. Phys.*, 2005, **68**, 743–798.
42 M.-C. Lu, R.-B. Wang, A. Yang and S. Duhm, *J. Phys.: Condens. Matter*, 2016, **28**, 094005.
43 N. Koch, A. Gerlach, S. Duhm, H. Glowatzki, G. Heimel, A. Vollmer, Y. Sakamoto, T. Suzuki, J. Zegenhagen, J. P. Rabe and F. Schreiber, *J. Am. Chem. Soc.*, 2008, **130**, 7300–7304.
44 W. H. Soe, C. Manzano, A. De Sarkar, N. Chandrasekhar and C. Joachim, *Phys. Rev. Lett.*, 2009, **102**, 176102.
45 N. Koch, A. Vollmer, S. Duhm, Y. Sakamoto and T. Suzuki, *Adv. Mater.*, 2007, **19**, 112–116.
46 N. Koch, *J. Phys.: Condens. Matter*, 2008, **20**, 184008.
47 E. Zojer, T. C. Taucher and O. T. Hofmann, *Adv. Mater. Interfaces*, 2019, **6**, 1900581.
48 A. Franco-Cañellas, S. Duhm, A. Gerlach and F. Schreiber, *Rep. Prog. Phys.*, 2020, **83**, 066501.
49 T.-L. Lee and D. A. Duncan, *Synchrotron Radiation News*, 2018, **31**, 16–22.
50 J. Zegenhagen, B. Detlefs, T.-L. Lee, S. Thiess, H. Isern, L. Petit, L. André, J. Roy, Y. Mi and I. Joumard, *J. Electron Spectrosc. Relat. Phenom.*, 2010, **178–179**, 258–267.
51 I. A. Vartanyants and J. Zegenhagen, *Solid State Commun.*, 1999, **113**, 299–320.
52 A. Gerlach, F. Schreiber, S. Sellner, H. Dosch, I. A. Vartanyants, B. C. C. Cowie, T. L. Lee and J. Zegenhagen, *Phys. Rev. B*, 2005, **71**, 205425.
53 G. van Straaten, M. Franke, F. C. Bocquet, F. S. Tautz and C. Kumpf, *J. Electron Spectrosc. Relat. Phenom.*, 2018, **222**, 106–116.
54 K. E. Hermann and M. A. Van Hove, *LEEDpat*, 2014, http://www.fhi-berlin.mpg.de/KHsoftware/LEEDpat/.
55 S. R. Forrest, *Chem. Rev.*, 1997, **97**, 1793–1896.
56 A. El-Sayed, P. Borghetti, E. Goiri, C. Rogero, L. Floreano, G. Lovat, D. J. Mowbray, J. L. Cabellos, Y. Wakayama, A. Rubio, J. E. Ortega and D. G. de Oteyza, *ACS Nano*, 2013, **7**, 6914–6920.
57 Y.-Y. Lo, J.-H. Chang, G. Hoffmann, W.-B. Su, C.-I. Wu and C.-S. Chang, *Jpn. J. Appl. Phys.*, 2013, **52**, 101601.
58 S. L. Wong, H. Huang, Y. L. Huang, Y. Z. Wang, X. Y. Gao, T. Suzuki, W. Chen and A. T. S. Wee, *J. Phys. Chem. C*, 2010, **114**, 9356–9361.
59 F. Evangelista, V. Carravetta, G. Stefani, B. Jansik, M. Alagia, S. Stranges and A. Ruocco, *J. Chem. Phys.*, 2007, **126**, 124709.
60 D. G. de Oteyza, A. Sakko, A. El-Sayed, E. Goiri, L. Floreano, A. Cossaro, J. M. Garcia-Lastra, A. Rubio and J. E. Ortega, *Phys. Rev. B*, 2012, **86**, 075469.

61 A. Franco-Cañellas, Q. Wang, K. Broch, B. Shen, A. Gerlach, H. F. Bettinger, S. Duhm and F. Schreiber, *Phys. Rev. Mater.*, 2018, **2**, 044002.
62 Q. Wang, M.-T. Chen, A. Franco-Cañellas, B. Shen, T. Geiger, H. F. Bettinger, F. Schreiber, I. Salzmann, A. Gerlach and S. Duhm, *Beilstein J. Nanotechnol.*, 2020, **11**, 1361–1370.
63 J. Zegenhagen, *Surf. Sci. Rep.*, 1993, **18**, 202–271.
64 A. Gerlach, C. Bürker, T. Hosokai and F. Schreiber, X-Ray Standing Waves and Surfaces X-Ray Scattering Studies of Molecule–Metal Interfaces, in *The Molecule–Metal Interface*, ed. N. Koch, N. Ueno and A. T. S. Wee, Wiley-VCH, Weinheim, Germany, 2013, pp. 153–172.
65 S. K. M. Henze, O. Bauer, T. L. Lee, M. Sokolowski and F. S. Tautz, *Surf. Sci.*, 2007, **601**, 1566–1573.
66 G. Heimel, S. Duhm, I. Salzmann, A. Gerlach, A. Strozecka, J. Niederhausen, C. Bürker, T. Hosokai, I. Fernandez-Torrente, G. Schulze, S. Winkler, A. Wilke, R. Schlesinger, J. Frisch, B. Bröker, A. Vollmer, B. Detlefs, J. Pflaum, S. Kera, K. J. Franke, N. Ueno, J. I. Pascual, F. Schreiber and N. Koch, *Nat. Chem.*, 2013, **5**, 187–194.
67 B. P. Klein, J. M. Morbec, M. Franke, K. K. Greulich, M. Sachs, S. Parhizkar, F. C. Bocquet, M. Schmid, S. J. Hall, R. J. Maurer, B. Meyer, R. Tonner, C. Kumpf, P. Kratzer and J. M. Gottfried, *J. Phys. Chem. C*, 2019, **123**, 29219–29230.
68 S. Duhm, S. Hosoumi, I. Salzmann, A. Gerlach, M. Oehzelt, B. Wedl, T.-L. Lee, F. Schreiber, N. Koch, N. Ueno and S. Kera, *Phys. Rev. B*, 2010, **81**, 045418.
69 P. T. P. Ryan, P. L. Lalaguna, F. Haag, M. M. Braim, P. Ding, D. J. Payne, J. V. Barth, T. L. Lee, D. P. Woodruff, F. Allegretti and D. A. Duncan, *Chem. Commun.*, 2020, **56**, 3681–3684.
70 C. Schmidt, T. Breuer, S. Wippermann, W. G. Schmidt and G. Witte, *J. Phys. Chem. C*, 2012, **116**, 24098–24106.
71 D. Käfer, L. Ruppel and G. Witte, *Phys. Rev. B*, 2007, **75**, 085309.
72 J. Götzen, C. H. Schwalb, C. Schmidt, G. Mette, M. Marks, U. Höfer and G. Witte, *Langmuir*, 2011, **27**, 993–999.
73 Q. Wang, A. Franco-Cañellas, J. Yang, J. Hausch, S. Struzek, M. Chen, P. K. Thakur, A. Gerlach, S. Duhm and F. Schreiber, *ACS Appl. Mater. Interfaces*, 2020, **12**, 14542–14551.
74 S. R. Kachel, P.-M. Dombrowski, T. Breuer, M. Gottfried and G. Witte, *Chem. Sci.*, 2021, **12**, 2575–2585.
75 K. Akaike, A. Onishi, Y. Wakayama and K. Kanai, *J. Phys. Chem. C*, 2019, **123**, 12242–12248.
76 X.-Q. Shi, Y. Li, M. A. Van Hove and R.-Q. Zhang, *J. Phys. Chem. C*, 2012, **116**, 23603–23607.
77 S. Smalley, P. Darancet, J. R. Guest and J. A. Smerdon, *J. Phys. Chem. C*, 2020, **124**, 653–658.
78 G. D'Avino, S. Duhm, R. G. Della Valle, G. Heimel, M. Oehzelt, S. Kera, N. Ueno, D. Beljonne and I. Salzmann, *Chem. Mater.*, 2020, **32**, 1261–1271.
79 E. Goiri, M. Matena, A. El-Sayed, J. Lobo-Checa, P. Borghetti, C. Rogero, B. Detlefs, J. Duvernay, J. E. Ortega and D. G. de Oteyza, *Phys. Rev. Lett.*, 2014, **112**, 117602.
80 B. Stadtmüller, D. Lüftner, M. Willenbockel, E. M. Reinisch, T. Sueyoshi, G. Koller, S. Soubatch, M. G. Ramsey, P. Puschnig, F. S. Tautz and C. Kumpf, *Nat. Commun.*, 2014, **5**, 3685.
81 K. Broch, U. Heinemeyer, A. Hinderhofer, F. Anger, R. Scholz, A. Gerlach and F. Schreiber, *Phys. Rev. B*, 2011, **83**, 245307.
82 G. Heimel, I. Salzmann, S. Duhm and N. Koch, *Chem. Mater.*, 2011, **23**, 359–377.
83 G. D'Avino, L. Muccioli, F. Castet, C. Poelking, D. Andrienko, Z. G. Soos, J. Cornil and D. Beljonne, *J. Phys.: Condens. Matter*, 2016, **28**, 433002.
84 M. Klues and G. Witte, *CrystEngComm*, 2018, **20**, 63–74.
85 S. Yanagisawa, *Jpn. J. Appl. Phys.*, 2020, **59**, 031002.
86 I. Salzmann, S. Duhm, G. Heimel, M. Oehzelt, R. Kniprath, R. L. Johnson, J. P. Rabe and N. Koch, *J. Am. Chem. Soc.*, 2008, **130**, 12870–12871.